Supplemental Information

Acknowledgements | We thank T. Lammermann (LSB, NIAID), C.A. Parent, and P.V. Afonso (LCMB, NCI), P.M. Murphy (LMI, NIAID), and J.H. Kehrl (LIR, NIAID) for helpful discussions and critical review of the manuscript. We thank R.J. Lefkowitz (Duke Medical Center) for the β-arrestin-2 deficient mice and J.H. Kehrl (LIR, NIAID) for the β-arrestin-1 deficient mice. We thank D. Einhaus (LISB, NIAID) for organizational support. We thank the NIAID Biological Imaging Section for use of their post-collection analysis software and computers. This research was supported by the Intramural Research Programs of NIAID and NIBIB, NIH.

Author Contributions | C.P.A., Y.M.Z., N.Y.M., M.M.S., and R.N.G. designed and performed the biological experiments and analyzed the data. C.P.A., Y.M.Z., M.M.S., and R.N.G. wrote the paper and N.Y.M. contributed to draft revisions. J.S.Y. and N.Y.M. assisted in device fabrication and gradient characterization experiments. T.P. contributed to data analysis. M.M.S. and R.N.G. are equally contributing co-corresponding authors.

Supplementary Figures:

Figure S1 (Related to Methods: Spatio-Temporal Chemokine Profiles) | Microfluidic system design.

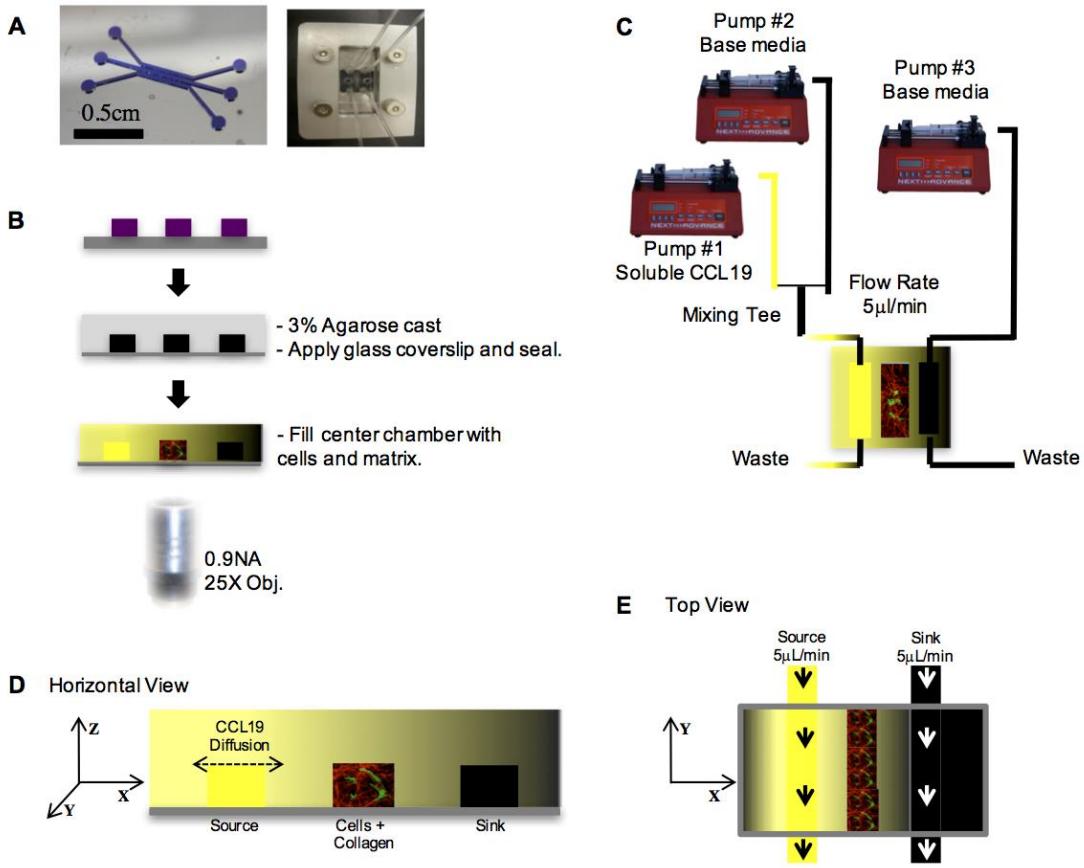

(A) Microfluidic 3-channel template (left) and assembled device including metal clamping plates with an acrylic manifold (right). **(B)** Scheme for agarose casting to form 3 channel device and subsequent fluorescent imaging. **(C)** Two programmable pumps in tandem with a downstream mixing tee were utilized to generate time-varying source concentrations. A third pump containing base medium maintained the sink channel at a constant chemokine concentration (effectively 0nM, except in presoak experiments). **(D)** Soluble chemokine diffused freely through the porous agarose barrier across the cell-matrix channel (with xyz-axis shown) and was removed via the sink channel. **(E)** Constant flow rates (5µl/min) were maintained in both the

source and sink channels (xy-axis shown).

Figure S2 (Related to Figure 1, Figure 2, and Methods) | Spatio-temporal gradient characterization of Alexa-Fluor 594-CCL19 and 10kDa-FITC dextran.

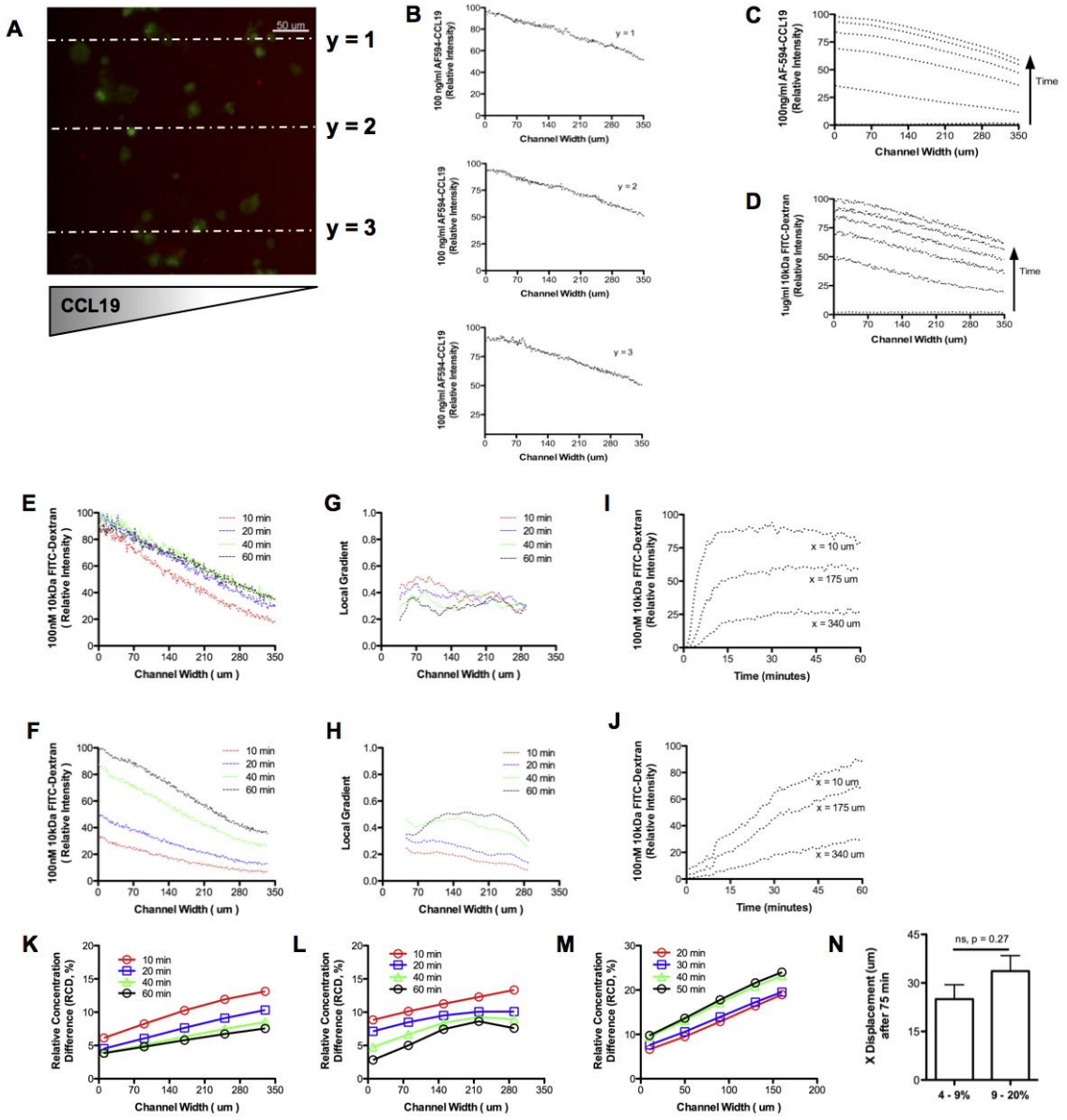

(A-B) Relative fluorescent intensity of AF594-CCL19 plotted across cell channel width (1-350μm) at various y positions. **(C)** Relative fluorescent intensity of Alexa-Fluor 594-CCL19 is compared with **(D)** 10kDa FITC-dextran plotted across channel width (1-350μm) for continuously rising source concentration. Relative fluorescent intensity of 10kDa-FITC dextran

(representing chemokine concentration) across channel width (1-350μm) at z = 100 μm for **(E)** stable and **(F)** continuously rising inputs. Corresponding local gradients across channel width (1-350μm) for **(G)** stable and **(H)** continuously rising inputs. Relative fluorescent intensity (representing chemokine concentration) over time at specific positions along the gradient (10μm, 175μm, 340μm) for **(I)** stable and **(J)** continuously rising inputs at z = 100 μm. Relative concentration difference (RCD) across a single cell width (20μm) varies with cell channel width. **(K)** RCD for stable source concentration in a wide channel (1-350μm). **(L)** RCD for continuously rising source concentration in a wide channel (1-350μm). **(M)** RCD in a medium channel with reduced width (1-200μm) for stable source concentration. **(N)** Comparison of the x-directed displacement for BMDCs exposed to stable CCL19 gradients in medium and wide channels, where channel width corresponds to gradient steepness: medium width (RCD = 4-9%) and large width (RCD = 9-20%), mean ± s.e.m.

Figure S3 (Related to Figure 1 and Figure 2) | Persistent directional BMDC migration requires a rising CCL19 gradient.

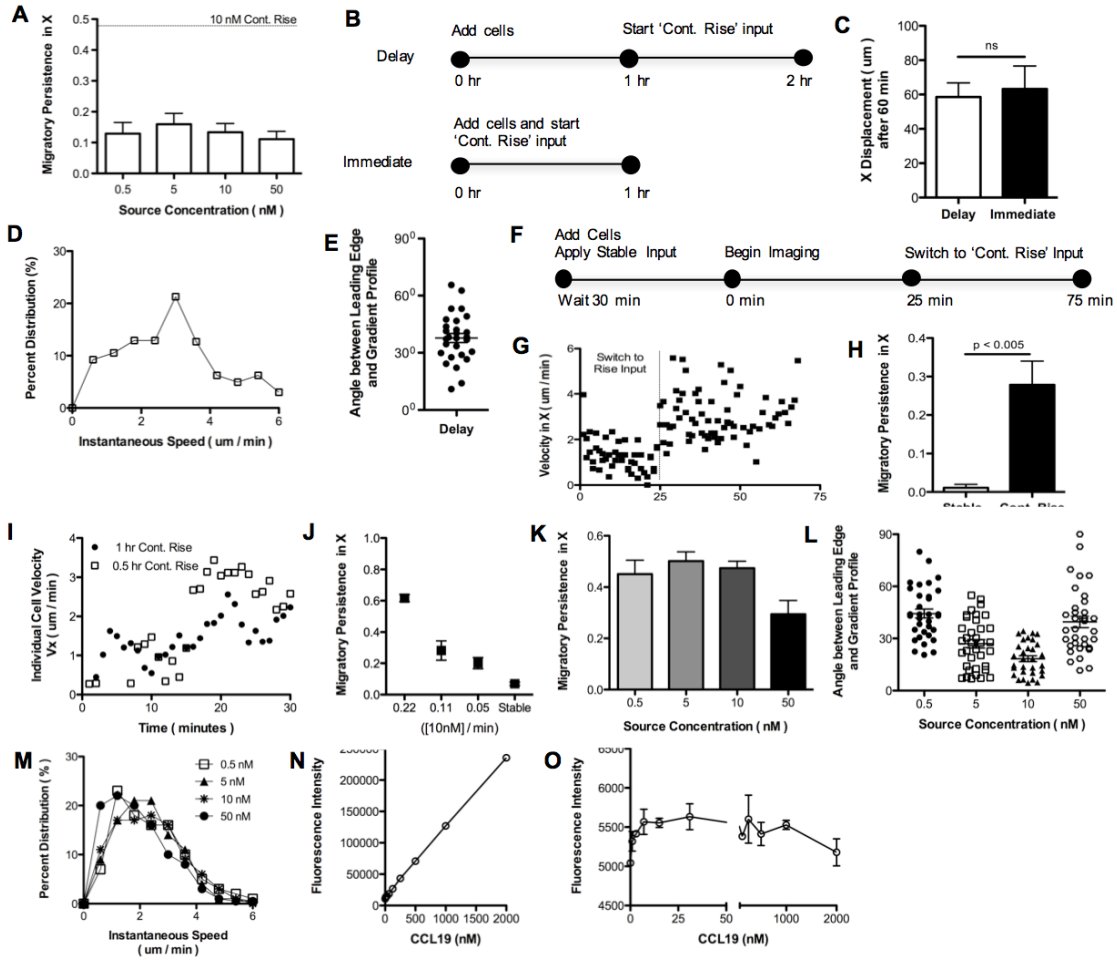

(A) Reduced chemotactic response of dendritic cells exposed to stable CCL19 input over a range of source concentrations (<<Kd to >> Kd). Representative data pooled from 2 experiments with ~8-10 measurements per group. Value of migratory persistence measured for continuously rising CCL19 input shown for reference. Dendritic cells incubated in microdevice for 1 hour prior to chemokine exposure ('Delay') show similar chemotactic responses compared with cells immediately exposed to chemokine gradients ('Immediate'). **(B)** Experimental scheme. **(C)** Total displacements along x-axis for cells exposed to delayed and immediate chemokine input. Each bar is representative of 4 experiments with ~10-20 cell tracks per group, mean ± s.e.m. **(D)** Histogram of instantaneous speeds across all cell tracks and all time points. Data pooled from 2 experiments with ~10-20 cell tracks per group. **(E)** Angle between the cell's leading edge and the

gradient axis measured from discrete images at 20 and 40 minutes following gradient input (0^0 = travelling toward, 90^0 = travelling perpendicular). Representative data pooled from 2 experiments with 8-10 measurements per group. Dendritic cells demonstrate robust chemotaxis when source chemokine is switched from stable to continuously rising input. **(F)** Experimental scheme. **(G)** Representative individual cell velocities across time. **(H)** Migratory persistence along x-axis for cells exposed to early stable input (0-25min) or to later continuously rising input (25-75min). Each bar is representative of 2 experiments with ~10-20 cell tracks per group, mean ± s.e.m. Dendritic cell speed and x-displacement correlate with rate of source concentration rise. **(I)** Source concentration increases from 0nM to 10nM over 0.5hr or 1hr. Representative individual cell velocities of migrating cells. **(J)** Migratory persistence along the x-axis across different rates for continuous source concentration rise. Source concentration increases from 0nM to 10nM over 45min, 90min, or 180min. Each dot (•) is an averaged value representative of 2 experiments with ~10-20 cell tracks per group. In rising chemokine fields, chemotaxis of dendritic cells correlates with bulk chemokine concentration. **(K)** Migratory persistence along spatial chemokine gradient for cells exposed to continuously rising source concentrations (0.5, 5, 10, 50 nM) for 60 minutes. Each bar is representative of 4 experiments with ~10-20 cell tracks per group. **(L)** Angle between the cell's leading edge and the gradient axis measured from discrete images at 20 and 40 minutes following gradient input (0^0 = travelling toward, 90^0 = travelling perpendicular). Representative data pooled from 2 experiments with 8-10 measurements per group. **(M)** Histogram of instantaneous speeds across all cell tracks and all time points. Data pooled from 4 experiments with ~10-20 cell tracks per group. **(N)** Mean fluorescent intensity of soluble calibration curve and **(O)** Elisa binding assay of custom tagged Alexa-Fluor 594 – CCL19. Data shown are representative of 3 individual experiments.

Figure S4 (Related to Figure 3 and Figure 4) | Grk3-mediated receptor desensitization determines temporal sensing requirement which is chemokine-specific.

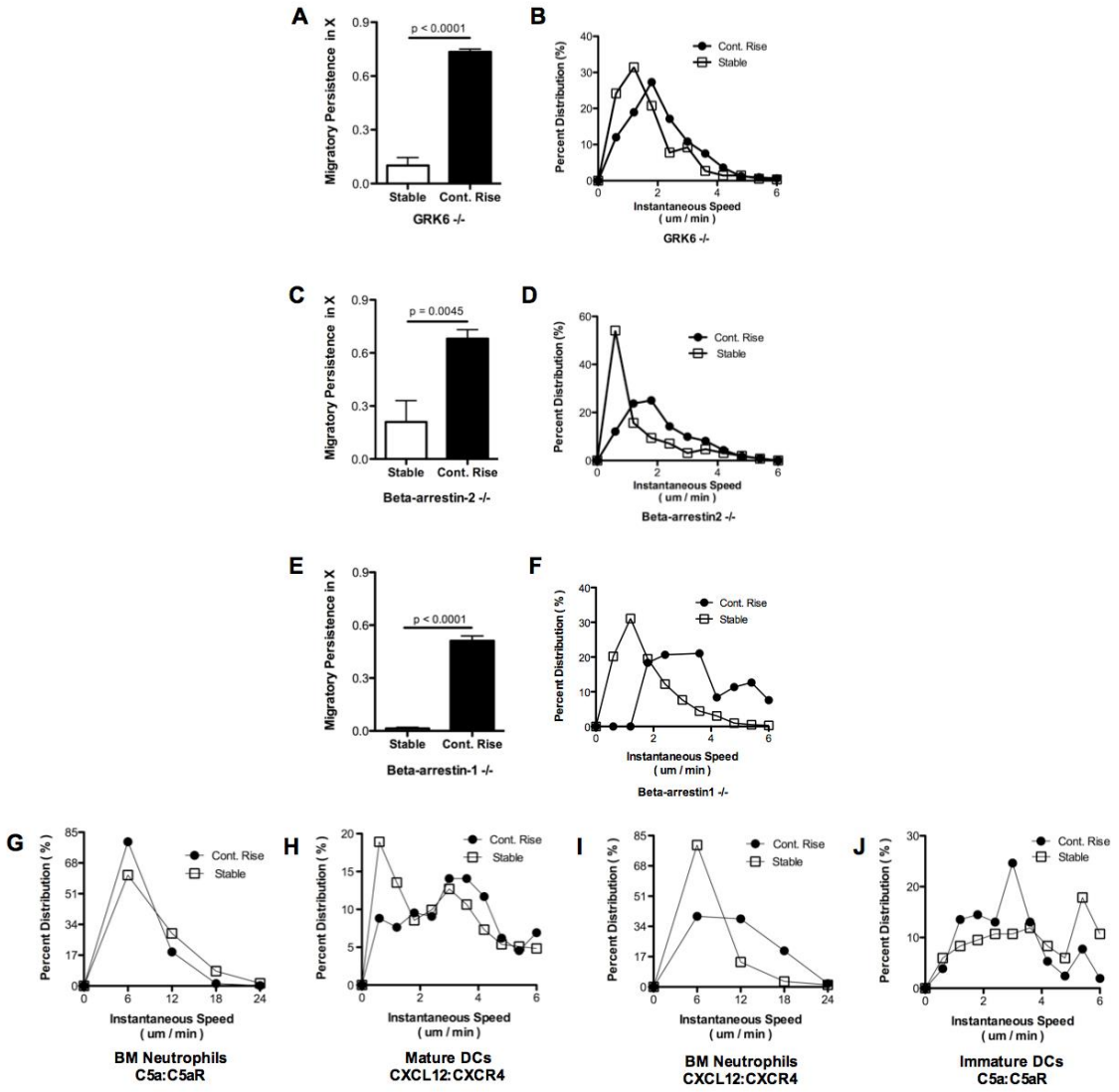

LPS-matured dendritic cells isolated from *Grk6*$^{-/-}$, β-arrestin-2$^{-/-}$, or β-arrestin-1$^{-/-}$ mice show similar chemotactic responses to WT cells. **(A, C, E)** Migratory persistence along x-axis of cells exposed to either stable or continuously rising source concentrations for 60 minutes. Each bar is representative of 2 experiments with ~10-20 cell tracks per group. **(B, D, F)** Histogram of instantaneous speeds across all cell tracks and all time points. Data pooled from 2 experiments

with ~10-20 cell tracks per group. Temporal sensing which drives persistent cellular migration is chemokine-specific. Chemotactic behavior of **(G, I)** freshly isolated neutrophils, **(H)** LPS-matured BMDCs (cultured 9 days), and **(J)** immature BMDCs (cultured 6 days) in response to stable or continuously rising source concentrations of CXCL12 **(H, I)** or C5a **(G, J)**. Histogram of instantaneous speeds across all cell tracks and all time points. Data pooled from 2 experiments with ~10-20 cell tracks per group.

Figure S5 (Related to Figure 5) | Early spatial cues (front-rear concentration differences) may dominate the initial direction of polarization in myeloid cells exposed to a homogeneous chemokine concentration for 10 minutes ('Homogeneous').

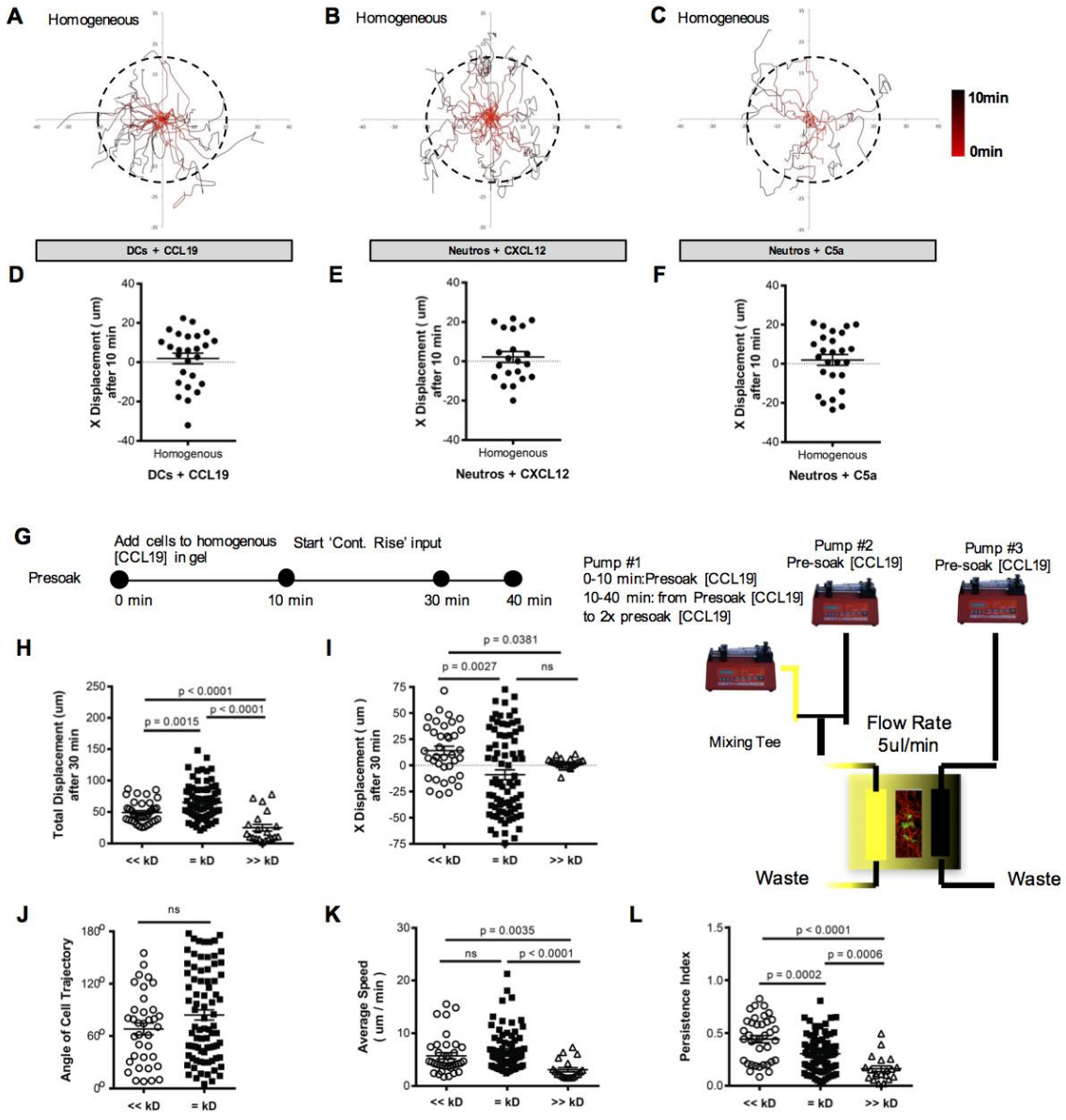

(A-C) Individual cell tracks plotted from a common starting coordinate with color scale bars (red to black, corresponding to 0 min to 10 min) indicating cell positions at specific times in the track. **(D-F)** X-displacement plotted along the spatial chemokine gradient. Dashed circle corresponds to a displacement of about 1-2 cell diameters from the initial starting position. Data are representative of 2 experiments with ~10 cell tracks per group. LPS-matured dendritic cells exposed to a homogeneous chemokine field of CCL19 (<<<Kd, = Kd, or >>>Kd) for 10 minutes followed by a continuously rising source, called "Presoak". **(G)** Experimental scheme. **(H)** Total

displacement, **(I)** x-displacement, **(J)** angle of cell trajectory measured from discrete images at 20 minutes following continuously rising gradient input (30 minutes total after start of image capture, as shown in figure), **(K)** average speed, and **(L)** persistence index during the continuously rising phase only. Each data point represents a single cell taken from 4 individual experiments with ~10-20 cell tracks per group, mean ± s.e.m.

Supplementary Movie Legends:

Movie S1 (Related to Experimental Setup) | Representative 3D rendering of cell – collagen channel. LPS-matured CD11c-eYFP BMDC (green) are uniformly seeded throughout the collagen matrix.

Movie S2 (Related to Figures 1, 2 and Suppl. Fig 3) | Representative chemotactic migration behavior or LPS-matured CD11c-YFP BMDC (green) in response to:

1. a stable source of CCL19,
2. a pre-set stable source of CCL19,
3. a stable source of CCL19 that switches to a continuously rising input at 30 minutes,
4. a continuously rising source of CCL19.

The soluble CCL19 gradient runs from left (source concentration) to right (base medium). Complete x-y-z stack (350 x 350 x 100 μm) imaged every 45 seconds utilizing a 0.9 NA 20X objective with a 510 Zeiss confocal microscope.

Movie S3 (Related to Figure 3) | Representative chemotactic behavior of LPS-matured

CD11c-YFP (green) and DsRed/*Grk3*$^{-/-}$ (Red) BMDC in response to

1. rising then stable source of CCL19,
2. continuously rising source of CCL19.

The soluble CCL19 gradient runs from left (source concentration) to right (base medium). Phase images are collected every 45 seconds utilizing a 0.9 NA 20X objective with a 510 Zeiss microscope. Quantified data reported in **Figure 3**.

Movie S4 (Related to Figure 4) | Representative chemotactic behavior of neutrophils in response to

1. a rising source of C5a,
2. a stable source of C5a.

The soluble C5a gradient runs from left (source concentration) to right (base medium). Phase images are collected every 20 seconds utilizing a 0.9 NA 20X objective with a 510 Zeiss microscope. Quantified data reported in **Figure 4**.

Movie S5 (Related to Figure 5) | Representative chemotactic behavior of

1. **LPS-matured CD11c-YFP BMDC (green) in response to a CCL19 continuously rising input following an initial homogeneous presoaking.** The soluble spatial CCL19 gradient runs from left (source concentration) to right (base medium). Complete x-y-z stack (350 x 350 x 100 μm) imaged every 45 seconds utilizing a 0.9 NA 20X objective with a 510 confocal microscope.
2. **neutrophils in response to a C5a continuously rising input following an initial homogeneous presoaking.** The soluble spatial C5a gradient runs from left (source

concentration) to right (base medium). Phase images are collected every 20 seconds utilizing a 0.9 NA 20X objective with a 510 Zeiss microscope.

Quantified data reported in **Figure 5**.

Movie S6 (Related to Figure 6) | Representative chemotactic behavior of WT and *Grk3*$^{-/-}$ BMDC in response to

1. a CCL19 continuously rising input following an initial homogeneous presoaking,
2. a CXCL12 continuously rising input following an initial homogeneous presoaking.

WT cells are shown in green, *Grk3*$^{-/-}$ cells in red. The soluble spatial CCL19 gradient runs from left (source concentration) to right (base medium). Complete x-y-z stack (350 x 350 x 100 μm) imaged every 45 seconds utilizing a 0.9 NA 20X objective with a 510 confocal microscope. Quantified data reported in **Figure 6**.